EFFECTS OF HELIX ANGLE VARIATIONS ON STABILITY OF LOW IMMERSION MILLING

B. Moetakef Imani, M. H. Sadeghi & M. Kazemi Nasrabadi

Abstract: *The stability behavior of low immersion helical end milling processes is investigated in this paper. Low radial immersion milling operations involve interrupted cutting which induces chatter vibration under certain cutting conditions. Time Finite Element Analysis (TFEA) is suggested for an approximate solution for delayed differential equations encountered during interrupted milling. An improved TFEA is proposed which includes the effects of helix angle variations on cutting force, cutting time and specific cutting force coefficients. For this purpose, five different cases were distinguished for engagement limits of the cutting edges. It has been observed that an increase in the helix angle improves the stability limit of the process. This is related to the flip bifurcation lobes that start to separate from the main lobes and shape isolated unstable islands. By further increasing the helix angle, unstable islands will vanish.*

1. Introduction

Milling is becoming an increasingly universal machining operation for producing parts used in aerospace, automotive, and life science engineering industries. The characteristics common to such parts are a high level of complexity and structural flexibility, both of which usually necessitate using low radial immersion milling operations. In addition, high speed milling (HSM) is vastly employed in order to increase material removal rate (MRR), improve surface finish and decrease the amount of cutting force [1].

Low radial immersion milling operations involve interrupted cutting which, in turn, induce chatter vibrations under certain cutting conditions. Davies et al. [2] proposed a single DOF model for low immersion milling simulation. They assumed that the time of cutting is short compared to the characteristic response time of the system (i.e., the position of the oscillator remains constant). Therefore, the system is simplified to a discrete map in the time domain. The stability analysis of the map reveals an additional stability region due to flip bifurcation. In a following study, Bylay et al proposed that the stability of interrupted cutting can be estimated by Temporal

B. Moetakef Imani, Assistant professor, Department of Mechanical Engineering, Ferdowsi University of Mashhad, Mashhad, Iran, bm_imani@yahoo.com

M.H.Sadeghi, Associate professor, Department of Mechanical Engineering, Tarbiat Modares University, Tehran, Iran, Sadeghim@modares.ac.ir

M.Kazemi Nasrabadi, Department of Aerospace Engineering, Shahid Sattari Air University, Tehran, Iran, m_nasr1350@yahoo.com

Finite Element Analysis (TFEA) [3]. This method is based on introducing finite elements in the time domain. The displacement and velocity at the end of each element is set equal to the displacement and velocity at the beginning of the next element while the cutting edge is engaged. The cutting force is also affected by the cutting edge displacement occurring one period earlier. TFEA introduces an approximate solution for the system [4]. The eigen-values of the proposed discrete linear map can anticipate the stability of milling operations.

Hartung et al. proposed using the semi-discretization (SD) method for turning and milling operations with single degree of freedom [5]. The semi-discretization is a well known technique in the finite element analysis of solid or fluid mechanics. The partial differential equation is only discretized along the spatial coordinates, leaving time unchanged. The semi-discretization of a delayed differential equation results in the time-delayed term being approximated by a piecewise constant function. Finally, the DDE is approximated by a series of ODE's. The discrete map is given as $y_{i+1} = B_i y_i$ and the stability properties are determined by the eigen-values of the Floquent transition matrix [6]. Insperger et al. investigated the effects of the helical cutting edge on the stability of interrupted cutting. The proposed method was based on the SD method which approximately solves the DDE equation. It was shown that the unstable flip region can be changed to flip islands as the helix angle increases [7].

The previous researches are limited either to the TFEA method with zero helix angle[7] or to SD method which can approximately include the helix angle

variation[6]. This study proposes using an improved TFEA method which can efficiently include the variation of helix angle in the method.

Henceforth, this paper is organized as follows: Section 2 demonstrates general milling mechanics and required definitions. TFEA relationships for the zero helix angle are explained in Section 3, after which the transition matrix for investigating stability behavior is derived. Section 4 includes the effect of the helix angle variation in the TFEA approach. Also, based on the engaged portion of the helical cutting edge, the cutting time formulations for the five different cases are derived. Two case studies are simulated by the improved TFEA approach in Section 5. The last section concludes the paper and proposes some areas for further work.

2. Milling Mechanics

A schematic diagram of the milling process is shown in Figure 1. The structure is assumed to have flexibility in the x-direction. Thus, the system can be treated as a single DOF vibratory model.
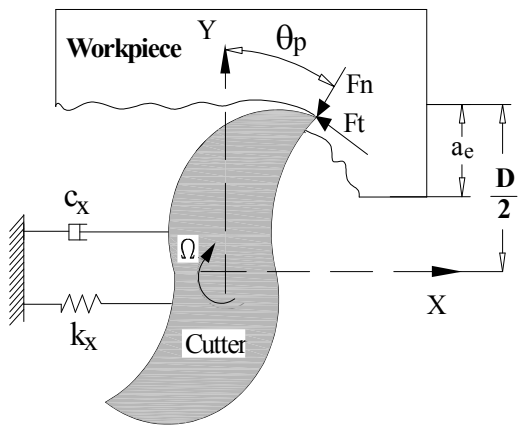

Fig. 1. Single DOF vibratory model of milling processes

The governing equation of motion is given as [6]:

$$m\ddot{x}(t) + c\dot{x}(t) + kx(t) = F_x(t) \tag{1}$$

where m, c, k are the mass, the damping and the stiffness parameters, respectively. F_x denotes the component of the cutting force in the x-direction for a zero helix cutter.

According to Figure 2, the x component of the cutting force on the p_{th} tooth is:

$$F_{xp}(t) = g_p(t)[-F_{tp}(t)\cos\theta_p(t) - F_{np}(t)\sin\theta_p(t)] \tag{2}$$

where $g_p(t)$ acts as a switching function. It is equal to 1 if the tooth is in-cut and 0 if it is not in-cut [8] and [9]. $\theta_p(t)$ denotes the cutting angle.
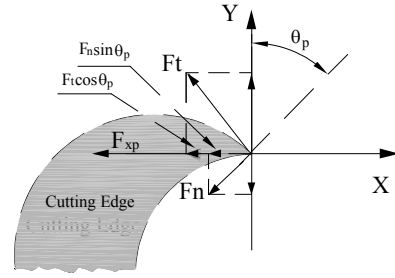

Fig. 2. Cutting force components for milling processes

The tangential and normal cutting force components can be approximated by [6]:

$$F_{tp}(t) = K_t.b.w_p(t) \tag{3}$$

$$F_{np}(t) = K_n.b.w_p(t) \tag{4}$$

where K_t and K_n are tangential and normal cutting coefficients, respectively. b represents the axial depth of cut (DOC) and $w_p(t)$ is the radial chip thickness which depends on the feed per tooth h. The regeneration of waviness is provided by the following relationship [10]:

$$w_p(t) = h\sin\theta_p(t) + [x(t) - x(t-\tau)]\sin\theta_p(t) \tag{5}$$

The cutting angle $\theta_p(t)$ can be computed by:

$$\theta_p(t) = \Omega t + 2\pi(p-1)/N , \\ p = 1, 2, 3, ..., N , \Omega = \frac{2\pi n}{60} \tag{6}$$

The tooth passing period is $\tau = \frac{60}{Nn}$, where N is the number of cutting edges and n is spindle speed given in rpm. Substitution of Equations (3 to 6) into Equation (2) yields the total cutting force acting in the x-direction:

$$F_{xp}(t) = \sum_{p=1}^{N} g_p(t)[-K_t b\cos\theta_p - K_n b\sin\theta_p]. \\ \{h\sin\theta_p(t) + [x(t) - x(t-\tau)]\sin\theta_p(t)\} \tag{7}$$

which can be simplified by the substitution of the following terms [10]:

$$K_c(t) = \sum_{p=1}^{N} g_p(t)[K_t\sin\theta_p(t)\cos\theta_p(t) + K_n\sin\theta_p(t)\sin\theta_p(t)] \tag{8}$$

$$f_\circ(t) = \sum_{p=1}^{N} h.g_p(t)[K_t\sin\theta_p(t)\cos\theta_p(t) + K_n\sin\theta_p(t)\sin\theta_p(t)] \tag{9}$$

Thus, the resulting equation of motion can be written in the following form:

$$m\ddot{x}(t) + c\dot{x}(t) + kx(t) = -bK_c(t)[x(t) - x(t-\tau)] - bf_\circ(t) \tag{10}$$

The above equation shows the standard delayed differential equation (DDE) for the milling process [10].

3. Time Finite Element Analysis

The dynamic behavior of the end milling process, which is considered to have flexibility along the x direction, is expressed by Equation (10). Since this equation does not have a closed form solution, an approximate solution is taken into consideration. One method which was proposed for the approximation solution of the above equation is Time Finite Element Analysis (TFEA) [11]. This method was first applied by Bayly et al. to the interrupted turning process [3]. In the following research, TFEA is also implemented for low immersion end-milling processes [12], but it was limited to the zero helix angles.

In low immersion milling with a one-, two- or multi-flute cutter, the tool switches between cutting and non-cutting phases. In the non-cutting phase, the system experiences free vibrations:

$$m\ddot{x}(t) + c\dot{x}(t) + kx(t) = 0 \tag{11}$$

This phase can be described by an exact closed form solution. In the cutting phase, the equation of motion is given by Equation (10). Because of the time-delayed term, there is no exact solution for this equation. TFEA divides the cutting time, t_c, into multiple elements and approximates the displacement vector on each element by a linear combination of polynomial trial functions [9], [10], [11] and [12].

3-1. Free Vibration Phase

The exact solution for the free vibration phase is given by the following relationship:

$$m\ddot{x}(t) + c\dot{x}(t) + kx(t) = 0 \tag{12}$$

where $\lambda_{1,2} = -\xi\omega_n \pm i\omega_d$ and $\omega_d = \omega_n\sqrt{1-\xi^2}$, ω_n is the natural frequency (rad/sec) and ξ is the damping ratio given by $\xi = \dfrac{c}{2\sqrt{km}}$. After the cutting edge leaves the material, the tool starts free vibrations with duration of t_f. Figure 3 depicts the contact face of the tool with the part. The length of contact is given by $\dfrac{D}{2}\theta_p$, where D is the tool diameter. The state translation matrix which relates the initial state of free vibration to the final state is derived as [3] and [13]:

$$\Phi = \frac{1}{\lambda_2 - \lambda_1}\begin{bmatrix} -\lambda_1 e^{\lambda_2 t_f} + \lambda_2 e^{\lambda_1 t_f} & -e^{\lambda_1 t_f} + e^{\lambda_2 t_f} \\ -\lambda_1\lambda_2 e^{\lambda_2 t_f} + \lambda_1\lambda_2 e^{\lambda_1 t_f} & -\lambda_1 e^{\lambda_1 t_f} + \lambda_2 e^{\lambda_2 t_f} \end{bmatrix},$$
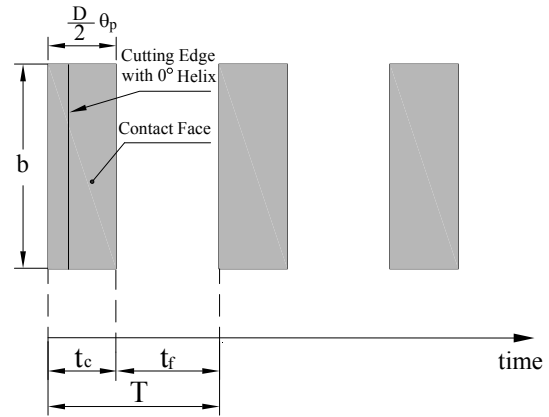$$\begin{Bmatrix} x(t_c + t_f) \\ \dot{x}(t_c + t_f) \end{Bmatrix} = \Phi\begin{Bmatrix} x(t_c) \\ \dot{x}(t_c) \end{Bmatrix} \tag{13}$$

Fig. 3. Contact face, cutting time t_c and non cutting time t_f for $0°$ helix

3-2. Vibration During Cutting Phase

The approximate solution for displacement during j_{th} element of the n_{th} period of engagement is given by [10]:

$$\mathbf{X}(t) = \sum_{i=1}^{4} \mathbf{a}_{ji}^n \phi_i(\sigma_j(t)) \tag{14}$$

where $\phi_i(\sigma_j(t))$ are Hemite trial functions defined by [3] and [10]:

$$\phi_1(\sigma_j) = 1 - 3(\frac{\sigma_j}{t_j})^2 + 2(\frac{\sigma_j}{t_j})^3$$
$$\phi_2(\sigma_j) = t_j[(\frac{\sigma_j}{t_j}) - 2(\frac{\sigma_j}{t_j})^2 + (\frac{\sigma_j}{t_j})^3]$$
$$\phi_3(\sigma_j) = 3(\frac{\sigma_j}{t_j})^2 - 2(\frac{\sigma_j}{t_j})^3 \tag{15}$$
$$\phi_4(\sigma_j) = t_j[-(\frac{\sigma_j}{t_j})^2 + (\frac{\sigma_j}{t_j})^3]$$

In the above relationship, $\sigma_j(t) = t - n\tau - \sum_{k=1}^{j-1} t_K$ represents the local time within the j_{th} element.

The initial and final displacement and the velocity of the j_{th} element are given as:

$$x(t_{0j}^n) = a_{j1}^n, \quad \dot{x}(t_{0j}^n) = a_{j2}^n \; (initial\ cond.)$$
$$x(t_{1j}^n) = a_{j3}^n, \quad \dot{x}(t_{1j}^n) = a_{j4}^n \; (final\ cond.) \tag{16}$$

At entry into the cut, x and $\dot{x}$ are expressed by the coefficients of the first two basis functions (i.e. a_{11}^n, a_{12}^n), respectively. Also, x and $\dot{x}$ at end of each element are equal to x and $\dot{x}$ at the start of the next element. For the last element, a_{j3}^n and a_{j4}^n represent the displacement and velocity of the tool as it leaves the cut. The weighted residual method defined in [14] is used to obtaine two more equations for each element.

Test functions are chosen as: $\psi_1(\sigma_j)=1$ and $\psi_2(\sigma_j)=\dfrac{\sigma_j}{t_j}-\dfrac{1}{2}$. The definite integral, which leads to two more equations, can be written as:

$$\int_0^{t_j}\left\{M\left(\sum_{i=1}^{4}\mathbf{a}_{ji}^{n}\ddot{\phi}_i(\sigma_j)\psi_p(\sigma_j)\right)\right.$$
$$+\mathbf{C}\left(\sum_{i=1}^{4}\mathbf{a}_{ji}^{n}\dot{\phi}_i(\sigma_j)\psi_p(\sigma_j)\right)$$
$$+(\mathbf{K}-b\mathbf{K}_c(\sigma_j))\left(\sum_{i=1}^{4}\mathbf{a}_{ji}^{n}\phi_i(\sigma_j)\psi_p(\sigma_j)\right) \qquad (17)$$
$$+bK_c(\sigma_j)\left(\sum_{i=1}^{4}\mathbf{a}_{ji}^{n-1}\phi_i(\sigma_j)\psi_p(\sigma_j)\right)$$
$$\left.-b\mathbf{f}_0(\sigma_j)\psi_p(\sigma_j)\right\}d\sigma_j=0 \qquad , \qquad p=1,2$$

The above equations can be represented by the following matrix equation for the j_{th} element:

$$\begin{bmatrix} N_{11} & N_{12} & N_{13} & N_{14} \\ N_{21} & N_{22} & N_{23} & N_{24} \end{bmatrix}\begin{Bmatrix} a_{j1} \\ a_{j2} \\ a_{j3} \\ a_{j4} \end{Bmatrix}^{n}=$$

$$\begin{Bmatrix} C_1 \\ C_2 \end{Bmatrix}+\begin{bmatrix} P_{11} & P_{12} & P_{13} & P_{14} \\ P_{21} & P_{22} & P_{23} & P_{24} \end{bmatrix}\begin{Bmatrix} a_{j1} \\ a_{j2} \\ a_{j3} \\ a_{j4} \end{Bmatrix}^{n-1} \qquad (18)$$

where N_{pi}, C_p and P_{pi} are given as:

$$N_{pi}=\int_0^{t_j}\left\{m\ddot{\phi}_i+c\dot{\phi}_i+(k+K_c b)\phi_i\right\}\psi_p d\sigma$$

$$C_p=\int_0^{t_j}bf_\circ\psi_p d\sigma \qquad (19)$$

$$P_{pi}=\int_0^{t_j}K_c b\phi_i\psi_p d\sigma$$

3-3. Transition Matrix

Initial and final conditions during free vibrations are related as follows [15]:

$$\begin{pmatrix} \mathbf{a}_{11} \\ \mathbf{a}_{12} \end{pmatrix}^{n}=\Phi\begin{pmatrix} \mathbf{a}_{E3} \\ \mathbf{a}_{E4} \end{pmatrix}^{n-1} \qquad (20)$$

E denotes the number of elements. The coefficients of the assumed solution can be obtained using the coefficients of the pervious period and a constant vector. The following matrix equation is written for E elements:

$$\begin{bmatrix} I & 0 & 0 & 0 & .... & 0 \\ N_1^1 & N_2^1 & 0 & 0 & .... & 0 \\ 0 & N_1^2 & N_2^2 & 0 & .... & 0 \\ ... & ... & ... & ... & .... & ... \\ ... & ... & .... & ... & .... & ... \\ ... & ... & ... & ... & ....N_1^E & N_2^E \end{bmatrix}\begin{Bmatrix} \begin{bmatrix} a_{11} \\ a_{12} \end{bmatrix} \\ \begin{bmatrix} a_{21} \\ a_{22} \end{bmatrix} \\ ... \\ \begin{bmatrix} a_{E3} \\ a_{E4} \end{bmatrix} \end{Bmatrix}^{n}=$$

$$\begin{bmatrix} 0 & 0 & 0 & 0 & .... & \Phi \\ P_1^1 & P_2^1 & 0 & 0 & .... & 0 \\ 0 & P_1^2 & P_2^2 & 0 & .... & 0 \\ ... & ... & ... & ... & .... & ... \\ ... & ... & ... & ... & .... & ... \\ ... & ... & ... & ... & ....P_1^E & P_2^E \end{bmatrix}\times\begin{Bmatrix} \begin{bmatrix} a_{11} \\ a_{12} \end{bmatrix} \\ \begin{bmatrix} a_{21} \\ a_{22} \end{bmatrix} \\ ..... \\ \begin{bmatrix} a_{E3} \\ a_{E4} \end{bmatrix} \end{Bmatrix}^{n-1}+\begin{Bmatrix} \begin{bmatrix} 0 \\ 0 \end{bmatrix} \\ \begin{bmatrix} C_1 \\ C_2 \end{bmatrix} \\ ...... \\ \begin{bmatrix} C_1 \\ C_2 \end{bmatrix} \end{Bmatrix}$$

$$(21)$$

where the sub-matrices are given as:

$$\mathbf{N}_1^j=\begin{bmatrix} N_{11}^j & N_{12}^j \\ N_{21}^j & N_{22}^j \end{bmatrix} \quad , \quad \mathbf{N}_2^j=\begin{bmatrix} N_{13}^j & N_{14}^j \\ N_{23}^j & N_{24}^j \end{bmatrix}$$

$$\mathbf{P}_1^j=\begin{bmatrix} P_{11}^j & P_{12}^j \\ P_{21}^j & P_{22}^j \end{bmatrix} \quad , \quad \mathbf{P}_2^j=\begin{bmatrix} P_{13}^j & P_{14}^j \\ P_{23}^j & P_{24}^j \end{bmatrix} \qquad (22)$$

The linear discrete map defined by Eq. (21) can be written as:

$$\mathbf{A}\,\mathbf{a}_n=\mathbf{B}\,\mathbf{a}_{n-1}+\mathbf{C} \qquad (23)$$

or

$$\mathbf{a}_n=\mathbf{Q}\,\mathbf{a}_{n-1}+\mathbf{D} \qquad (24)$$

The eigen-values of the transition matrix $Q=A^{-1}B$ will determine the stability of the system. If the magnitude of any eigen-value exceeds 1, then the solution with given parameters is unstable.

4. Effects of Helix Angle Variation on Stability

The main objective of this research is to investigate the effects of the helix angle variation on the stability of low immersion milling operations. In this regard, the TFEA approach is enhanced in order to take into account the variation of the helix angle in the formulation.

4-1. Cutting Force Calculation Including Helix Angle Effect

For an end-mill with a helix angle of β, the cutting force along the x direction (Fx), can be written as: [16]

$$F_x(t)=\int_{z_1(t)}^{z_2(t)}dF_x(z,t) \qquad (25)$$

where $dF_x(z,t)$ is the differential force acting on the cutting edge element at z level. $z_1(t)$ and $z_2(t)$ are z-coordinates of the start- and end-point of engagement. The differential cutting force, dFx is given as:

$$dF_x(z,t) = -g_p(t)(dF_t \cos\theta_p(z,t) + dF_n \sin\theta_p(z,t)) \tag{26}$$

where $\theta_p(z,t) = \Omega t - (\frac{2\tan\beta}{D})z$ and

$$dF_t = g(z,t).K_t.w(\theta(z,t)).dz \tag{27}$$

$$dF_n = g(z,t).K_n.w(\theta(z,t)).dz \tag{28}$$

The chip thickness is computed by:

$$w(\theta(z,t)) = h\sin\theta_p(z,t) + [x(t) + x(t-\tau)]\sin\theta_p(z,t) \tag{29}$$

Finally, the improved $K_c(t)$ and $f_o(t)$ can be written as:

$$K_c(t) = \sum_{p=1}^{N} g_p(t) \int_{z_1(t)}^{z_2(t)} [K_t \sin\theta_p(t)\cos\theta_p(t) + K_n \sin\theta_p(t)\sin\theta_p(t)]dz \tag{30}$$

$$f_o(t) = \sum_{p=1}^{N} h.g_p(t) \int_{z_1(t)}^{z_2(t)} [K_t \sin\theta_p(t)\cos\theta_p(t) + K_n \sin\theta_p(t)\sin\theta_p(t)]dz \tag{31}$$

4-2. Cutting Time Including Helix Angle Effect

Due to the inclination of the cutting edge introduced by the helix angle, the amount of time spent during cutting increases. See Figure 4 for details. The cutting t_c can be obtained by:

$$t_c = (\frac{D}{2}\theta_p + \frac{2\tan\beta}{D}b)/\Omega \tag{32}$$
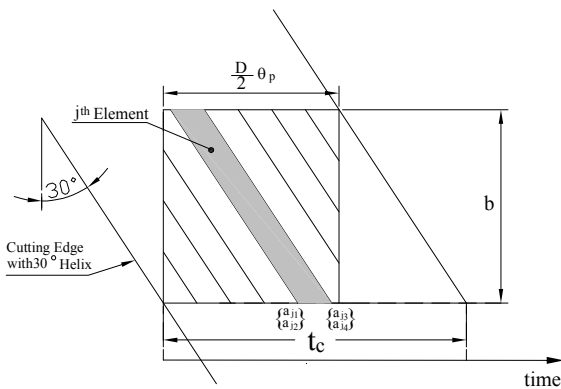

Fig. 4. Cutting time for helical end mills

4-3. Different Regions on Contact Face

The limits of integration, $z_1(t)$ and $z_2(t)$, depend on the tool diameter (D), helix angle (β), radial depth of cut (a_e) and axial depth of cut (b). Thus, the

following cases can be differentiated [16]. See Figure 5.

Case 0:

$$at \ z = 0, \ if \ \phi_{st} < \phi_j < \phi_{ex} \quad Then \quad z_{j,1} = 0$$
$$at \ z = b, \ if \ \phi_{st} < \phi_j < \phi_{ex} \quad Then \quad z_{j,2} = b \tag{33}$$

Case 1:

$$\begin{cases} at \ z = 0, \ if \ \phi_{st} < \phi_j < \phi_{ex} \quad then \ z_{j,1} = 0 \\ at \ z = b, \ if \ \phi_j < \phi_{st} \quad then \ z_{j,2} = \frac{1}{k_\beta}(\phi - \phi_{st}) \ , \ k_\beta = \frac{2\tan\beta}{D} \end{cases} \tag{34}$$

Case 2:

$$\begin{cases} at \ z = 0, \ if \ \phi_j > \phi_{ex} \ and \ at \ z = b, \ if \ \phi_{st} < \phi_j < \phi_{ex} \ Then \\ z_{j,1} = \frac{1}{k_\beta}(\phi - \phi_{ex}) \ , \ z_{j,2} = b \end{cases} \tag{35}$$

Case 3:

$$\begin{cases} at \ z = 0, \ if \ \phi_j > \phi_{ex} \ and \ at \ z = b, \ if \ \phi_j < \phi_{ex}, \phi_j < \phi_{st}, \\ then \quad z_{j,1} = \frac{1}{k_\beta}(\phi - \phi_{ex}) \ , \ z_{j,2} = \frac{1}{k_\beta}(\phi - \phi_{st}) \end{cases} \tag{36}$$

Case 4:

$$\begin{cases} at \ z = 0, \ if \ \phi_j > \phi_{ex} \ and \ at \ z = b, \ if \ \phi_j > \phi_{ex} \quad then \\ The \ flute \ is \ out \ of \ cut \end{cases} \tag{37}$$

The above mentioned parameters (i.e. D, β, a_e and b) can largely affect the variation of $K_c(t)$.
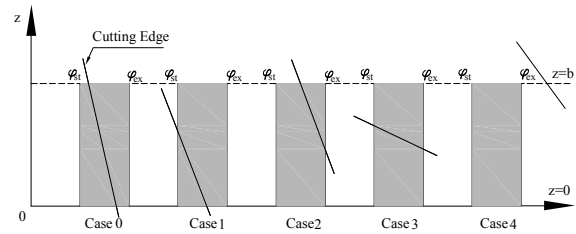

Fig. 5. Helical flute-part face integration zones

4-4. Specific Cutting Force Variation

Figure 6 presents the specific cutting force variation, $K_c(t)$, for a one fluted tool with a helix angle of 0° and 30°. The variations are computed for up milling at 10% and 50% immersions. The discontinuity of the function is due to interrupted cutting. As can be seen in the case of 10% immersion, the time spent in the cutting phase is much shorter than that spent in the free vibration phase. Thus, the traditional stability analysis proposed by [6] is not valid [6].

The following experimentally identified parameters were used for calculation of $K_c(t)$ [6]:

$$K_t = 5.5 \times 10^8 \ N/m^2 \ , \ K_n = 2 \times 10^6 \ N/m^2$$

As witnessed in Figure 6, the variation of the specific cutting force for the low immersion case (i.e. 10%

immersion) is smoother for the $30°$ helix angle. In addition, at the boundaries of engagement, the values of discontinuity are smaller for $30°$ helix angle.
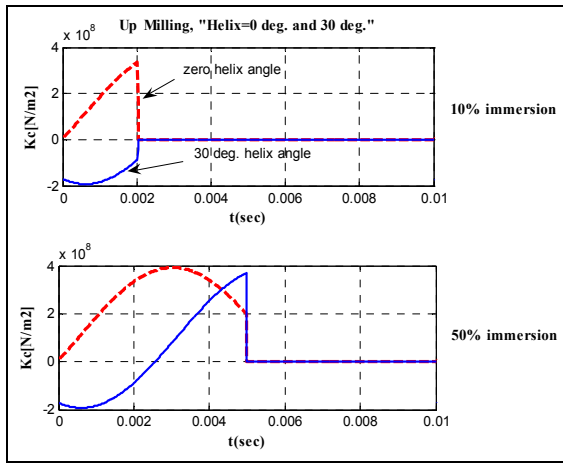

Fig. 6. Specific cutting force variation

5. TFEA Simulations

In order to investigate the effect of increasing the helix angle on the stability of low immersion milling, two previously confirmed cases are taken into consideration.

Case 1: The dynamic parameters of tool structure, cutting coefficients, tool diameter, helix angle and immersion are selected according to [6] and reported in Table 1.

Tab. 1. Selected System Parameters [6]

Modal Parameters for Single DOF	$m = 2.573\,kg$ $k = 2.18 \times 10^6\,N/m$ $c = 15.157\,\frac{N}{m/sec}$
Cutting Coefficient	$K_t = 6 \times 10^8\,N/m^2$ $K_n = 2 \times 10^8\,N/m^2$
Tool Parameters	$helix\ angle(\beta) =$ $0°, 30°, 45°, 60°$ Tool Diameter (d) = 12.7mm $aD = \dfrac{a_e}{D} = 0.1$ (10% Immersion)

Figure 7-(a) illustrates the stability lobs for a zero helix angle.

There are two types of stability lobes. the ones related to secondary Hopf bifurcation, and the ones related to period doubling (or flip) bifurcations. These lobes are referred to as Hopf lobes and flip lobes, respectively.

A flip bifurcation or period doubling phenomenon occurs when the negative real eigenvalue passes through -1; (2) a Hopf bifurcation occurs when a complex eigenvalue obtains a magnitude greater than 1.

The developed TFEA simulations are in agreement with the results given in [6]. Figures 7-(b) and -(c)

illustrate the effects of increasing the helix angle as anticipated by the proposed method. As observed, with the introduction of the helix angle the stability of the operation improves. By further increasing the helix angle, $\beta = 60°$ (see Figure 7(d)), the flip bifurcation will change to unstable islands as predicted by [7] using a different approach. The introduction of the helix angle will decrease the effect of impact at the boundary of engagement for low immersions. Thus, it is anticipated that non-zero helix angle will improve the stability of low immersion milling process which is confirmed by TFEA simulation.
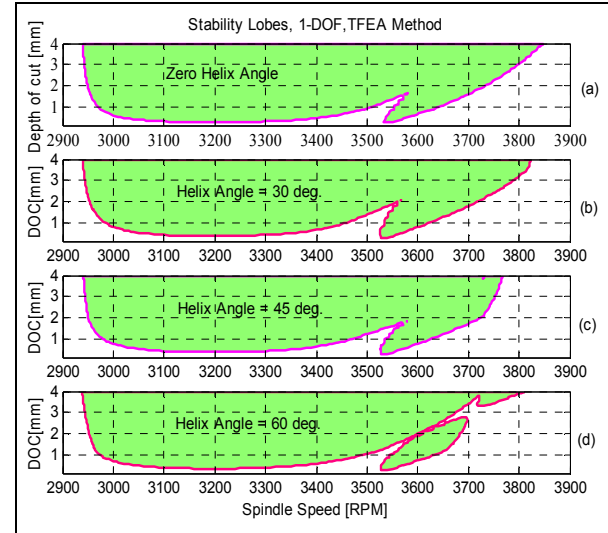

Fig. 7. Stability lobs for up-milling with radial immersion 10% and various helix angles

Case 2: The dynamic parameters of the tool/structure, cutting coefficients, and tool diameter are selected according to [7] and reported in Table 2.

Tab. 2. Selected System Parameters [7]

Modal Parameters for Single DOF	$m = 5.364\,kg$ $k = 21.6 \times 10^6\,N/m$ $c = 421.948\,\frac{N}{m/sec}$
Cutting Coefficient	$K_t = 804.3 \times 10^6\,N/m^2$ $K_n = 331 \times 10^6\,N/m^2$
Tool Parameters	$helix\ angle(\beta) =$ $0°, 10°, 30°, 45°$ Tool Diameter (d)= 20mm $aD = \dfrac{a_e}{D} = \dfrac{1}{20}$ (5% Immersion)

The immersion employed for all simulations is equal to 5%. For a maximum axial depth of cut 50mm and maximum helix angle of $45°$, only one edge of the two flute cutter is engaged during the cutting phase. The spindle speed range is 3000 rpm to 8500 rpm.

By increasing the helix angle, the flip bifurcation lobs will first change to unstable islands, By further increasing the helix angle, the islands will vanish (see Figure 8). Similar trends were observed by [7].
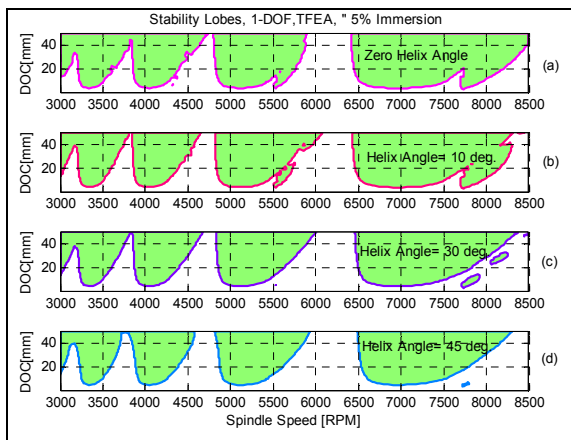

Fig. 8. Stability charts for up-milling with radial immersion 5% and various helix angles

6. Conclusion

In this research, the TFEA method has been enhanced to include the effects of helix angle variations. The cutting force, cutting time and specific cutting force variations have been calculated for helical end mills. Additionally, five different cases are differentiated and included in improved TFEA simulations. The validity of proposed method is confirmed by the results reported in [6] and [7]. This research proves that increasing the helix angle improves the stability of the milling process and change the flip bifurcation lobs into unstable islands. Moreover, by further augmenting the helix angle, the unstable islands vanish. In Case 1, for zero helix angle the results of the proposed TFEA complies completely with the results given in [7]. For non-zero helix angle (30°, 45° and 60°), the improve TFEA method illustrates the formation of unstable islands. There is no result reported for non-zero helix angles in [7]. In Case 2, the efficient TFEA method, developed in the current work, is compared with the SD method reported in [8] which is limited to none standard helix angles. The improved TFEA method is implemented for helix angle of 10°, 30° and 45°. The trend of stability lobes and the number of unstable islands are similar.

The realistic model for milling operations is a two DOF vibratory system which will be addressed in future work.

References

[1] Caulfield, F.L., *Electromechanical Actuator Development for Integrated Chatter Prediction on High Speed machining Centers.* Master of Science Dissertation, University of North Carolina, 2002.

[2] Davies, M.A., Pratt, J.R., Dutterer, B., Burns, T.J., *Stability Prediction for Low Radial Immersion Milling. Transactions of the ASME,* Journal of Manufacturing Science and Engineering. 124, 2002, pp. 217–225.

[3] Bayly, P.V., Halley, J.E., Mann, B.P., Davies, M.A., *Stability of Interrupted Cutting by Temporal Finite Element Analysis.* Transactions of the ASME, Journal of Manufacturing Science and Engineering. 125, 2003, pp. 220-225.

[4] Bayly, P.V., Mann, B.P., Davies, M.A., Pratt, J.R., *Stability analysis of interrupted cutting with finite time in the cut. Proceedings of ASME Design Engineering Technical Conference,* Manufacturing in Engineering Division, Orlando, FL. MED-11, 2000, pp. 989 -996.

[5] Hartung, F., Insperger, T., Stepan, G., Turi, J., *Approximate Stability Charts for Milling Processes using Semi-Discretization.* Applied Mathematics and Computation. 174, 2006, pp. 51- 73.

[6] Insperger, T., Mann, B.P., Stepan, G., Bayly, P.V., *Stability of Up-Milling and Down-Milling, Part1: Alternative Analytical Methods.* International Journal of Machine Tools and Manufacture. 43, 2003, pp. 25-34

[7] Insperger, T., Muñoa, J., Zatarain, M., Peigné, G., *Unstable Islands in the Stability Chart of Milling Processes Due to the Helix Angle.* CIRP 2nd Int. Conference High Performance Cutting. June 12-13, Vancouver, BC, Canada. 2006

[8]. Minis, I., Yanushevsky, R., *A New Theoretical Approach for the Prediction of Machine Tool chatter in Milling.* Journal of Engineering for Industry. 115, 1993, pp. 1–8.

[9]. Altintas, Y., Budak, E., *Analytical Prediction of Stability Lobes in Milling.* Annals of the CIRP. 44, 1995, pp. 357–362.

[10]. Mann, B.P., Bayly, P.V., Davies, M.A., Halley, J.E., *Limit Cycles, Bifurcations, and Accuracy of the Milling Process.* Journal of Sound and Vibration. 277, 2004, pp. 31-48.

[11] Gradisek, J., Govekar, E., Grabec, I., Kalveram, M., Weinert, K., Insperger, T., Ste'pan, G., *On Stability Prediction for Low Radial Immersion Milling.* Journal of Machine Science and Technology. 9, 2005, pp. 117–130.

[12] Bayly, P.V., Schmitz, T.L., Mann, B.P., Peters, D.A., Stepan, G., Insperger, T., *Effects of Radial Immersion and Cutting Direction on Chatter Instability in End Milling. Proceedings of IMECE.,* ASME International Mechanical Engineering Congress & Exposition., November 17-22. New Orleans, Louisiana, 2002.

[13] Mann, B. P., Young, K. A., Schmitz, T. L. and Dilley, D. N., Simultaneous Stability and Surface Location Error Predictions in Milling. Transactions of the ASME, Journal of Manufacturing Science and Engineering. 127, 2005, pp. 446-453.

[14] Peters, D. A. and Idzapanah, A.P., Hp-version finite elements for the space-time domain. Computational Mechanics 3, 1988, pp. 73-78.

[15] Mann, B.P., Young, K.A., Schmitz, T.L., Bartow, M.J., Bayly, P.V., *Machining Accuracy due to Tool or Workpiece Vibration.* Proceedings of IMECE, ASME International Mechanical Engineering Congress and Exposition, November 15-21, Washington, D.C. USA, 2003.

[16] Altintas, Y., *Manufacturing Automation: Metal Cutting Mechanics,* Machine Tool Vibration, and CNC Design. Cambridge University Press,. 2000